Pre-print submitted to ChemPhysChem

Published after as: ChemPhysChem (2016), 17 p. 1062-1069

Structural and electrochemical study of Vanadium doped TiO_2 ramsdellite with superior lithium storage properties for Li-ion batteries

Juan Carlos Pérez-Flores[a], Markus Hoelzel[b], Flaviano García-Alvarado[a],

Alois Kuhn*[,a]

[a] Departamento de Química y Bioquímica, Facultad de Farmacia, Universidad CEU San Pablo, 28668 Boadilla del Monte, Madrid, Spain

[b] Forschungsneutronenquelle Heinz Maier-Leibnitz (FRM II), Technische Universität München, Lichtenbergstr. 1, D-85747 Garching, Germany

*corresponding author

Ctra. Boadilla del Monte km. 5,300

28668 Boadilla del Monte, Madrid

SPAIN

Phone: (0034) 913724735

Fax: (0034) 913510475

E-mail: akuhn@ceu.es

Abstract

Titanium oxide-based materials are considered attractive and safe alternatives to carbonaceous anodes in Li-ion batteries. In particular the ramsdellite form TiO_2(R) is known for its superior lithium storage ability as bulk material when compared to other titanates. In this work we have prepared V-doped lithium titanate ramsdellites with formula $Li_{0.5}Ti_{1-x}V_xO_2$ ($0 \leq x \leq 0.5$) by a conventional solid state reaction. The lithium-free $Ti_{1-x}V_xO_2$ compounds, in which the ramsdellite framework remains virtually unaltered, are easily obtained by a simple aqueous oxidation-ion extraction process. Powder neutron diffraction is used to locate the Li channel site in $Li_{0.5}Ti_{1-x}V_xO_2$ compounds and to follow the lithium extraction by difference-Fourier maps. Previously delithiated $Ti_{1-x}V_xO_2$ ramsdellites are able to insert up to 0.8 Li^+ per transition metal. Initial gravimetric capacities of 270 mAh g^{-1} with good cycle stability under constant current discharge conditions are among the highest reported for bulk TiO_2-related intercalation compounds for the threshold of 1 e^- / formula unit.

Keywords: TiO_2, $Li_{0.5}Ti_{1-x}V_xO_2$, $Ti_{1-x}V_xO_2$, ramsdellite, titanate, lithium batteries, lithium-ion batteries, anode

1. Introduction

Titanates are being intensively investigated as anode materials for lithium-ion batteries due to their superior safety and rate capability compared with current state-of-art graphite.[1-8] Good reversibility was demonstrated for the Ti^{4+}/Ti^{3+} redox couple acting at a relative high operating voltage of typically 1.5V versus lithium in these cheap and nontoxic Ti-containing materials, which are thought to provide safer applications. $Li_4Ti_5O_{12}$ (LTO), the x = ⅓ end member of the $Li_{1+x}Ti_{2-x}O_4$ spinel solid solution system ($0 \le x \le ⅓$) [9], is now used in commercial lithium-ion batteries.[10] Spinel $LiTi_2O_4$ (the x=0 member in the $Li_{1+x}Ti_{2-x}O_4$ series) was observed to convert to $LiTi_2O_4$ with ramsdellite structure at high temperature.[11] Akimoto et al. solved the crystal structure of $LiTi_2O_4$(R) [12] and the delithiated TiO_2(R) polymorph [13] using single crystal diffraction data, and Gover et al. studied the transformation of spinel to ramsdellite by means of neutron diffraction data.[14] $LiTi_2O_4$(R) (or $Li_{0.5}TiO_2$(R)) and the corresponding Li-deinserted form, i.e. ramsdellite TiO_2(R), have attracted growing attention due to its superior Li insertion properties as the anode for Li rechargeable batteries.[15-17] TiO_2(R) with a theoretical specific capacity of 335 $mAhg^{-1}$, involving complete $Ti^{4+} \rightarrow Ti^{3+}$ reduction, practically doubles that of commercialized spinel $Li_4Ti_5O_{12}$ (175 mAh g^{-1}). TiO_2(R), besides

TiO_2(B), can accommodate more lithium than any other TiO_2 polymorph as a bulk material, although comparable high capacities can be achieved for those other forms by increasing the electrochemically active surface, i.e. downsizing particles to the nanoscale[18-20]. In addition, nanoparticulate forms of TiO_2(B) enhance rate capability compared to the bulk material.[18,21,22] Taking the existence of the mixed spinel systems $LiTi_{2-x}V_xO_4$ ($0 \leq x \leq 1$) and $LiTiCrO_4$ [5,23] as a basis, the formation of analogue mixed high temperature ramsdellite phases is expected to ocurr. A computational study of the spinel (Sp) to ramsdellite (R) transformation for several lithium titanates with composition $LiMTiO_4$ has been reported for M = V, Cr, Mn and Fe [24], and the thermal Sp $\rightarrow$ R transformation has been observed for $LiCrTiO_4$ [25] and $LiTi_{2-y}V_yO_4$ [26] at T > 1000ºC.

In this work the synthesis of $Li_{0.5}Ti_{1-x}V_xO_2$(R) and the respective delithiated $Ti_{1-x}V_xO_2$(R) within the compositional range $0 \leq x \leq 0.5$ is presented. We have determined the crystal structure of $Li_{0.5}Ti_{1-x}V_xO_2$ ramsdellites and its delithiated analogues by means of Rietveld analysis of powder X-ray and neutron diffraction data. These new materials are further characterized by microanalysis, thermogravimetric analysis, and finally their good electrochemical lithium insertion properties are examined in the light of their crystal structure.

2. Experimental Section

Crystalline $Li_{0.5}Ti_{1-x}V_xO_2$(R) in the compositional range $0 \leq x \leq 0.5$ was prepared by a conventional solid-state reaction as previously described.[26] Powder mixtures containing appropriate amounts of high purity TiO_2 (anatase, Sigma Aldrich, 99%), Ti_2O_3 (Sigma Aldrich, 99.8%), V_2O_3 (Sigma Aldrich, 99.8%) and Li_2TiO_3 were loaded into silica ampoules and sealed under dynamic vacuum (10^{-2} mbar). Li_2TiO_3 itself was previously prepared by reaction of Li_2CO_3 (Sigma Aldrich, 99.8%) and TiO_2 at 700°C. Reaction

mixtures were heated for two days to temperatures ranging from 950º C to 1050º C, depending on the vanadium content (x). Products were finely quenched to room temperature.

The delithiated ramsdellite forms were prepared by a combined ion extraction/oxidation process. In a typical treatment 1g $Li_{0.5}Ti_{1-x}V_xO_2$ was stirred in 50 mL of 1M HCl for 48 h. The powder was vacuum filtered, washed with small amounts of a 1:1 mixture of deionized water and ethanol, and dried at 80ºC under vacuum for 24 h to remove remaining solvents.

The successful complete lithium ion extraction was calculated by determining the lithium content in the filtered solution. Analysis of Li content was carried out by means of flame atomic emission spectroscopy, using a Sherwood 410 flame photometer and a standard lithium solution ($[Li^+]$ = 1000 ppm in HNO_3, Fluka). Completeness of lithium extraction was further confirmed by neutron diffraction (see below).

X-ray diffraction patterns of powder samples were recorded with $CuK_{\alpha 1}$ radiation (λ = 1.54056 Å) in transmission mode in a Siemens D5000 diffractometer, operated at 40 kV and 30 mA, equipped with a hybrid monochromator and a scintillation detector. For X-ray diffraction measurements finely ground and sieved ramsdellite powder (particle size < 50 μm) was spread onto a circular Mylar foil that was previously prepared with a thin film of Lithilen® high vacuum grease, and finally sandwiched with a second circular Mylar foil. All preparations were done in an Ar-filled glove box, owing to the air sensitivity of lithiated ramsdellites containing lower valent transition metals, such as Ti^{3+} and V^{3+}. Unit cell parameters of the $Li_{0.5}Ti_{1-x}V_xO_2$ samples, with x = 0 - 0.5, were determined with the Fullprof package.[27] Neutron powder diffraction (NPD) patterns of two selected samples (x=0 and 0.3) were collected on the high resolution SPODI diffractometer at the neutron reactor FRM II (Heinz Maier Leibnitz Zentrum, Garching

near Munich, Germany).[28] A Ge(551) monochromator was used to select a wavelength of λ = 1.5481 Å. A cylindrical vanadium can of 8 mm diameter was filled with 4g of ramsdellite powder sample. ND patterns were collected for 4h over the 2θ = 5-160º range with a step size of 0.05º at 298 K.

In structural analysis carried out with the Rietveld method [29] a pseudo-Voigt function was chosen to reproduce the line-shape of diffraction peaks. The coherent neutron scattering lengths used were: Li: –1.90 fm; Ti: –3.30 fm and O: +5.80 fm.[30] The negative length factors of the Ti and Li atoms increase considerably the contrast of Ti and light O and Li elements, enabling Fourier map investigations addressed to localize Li atoms.

Structural models were drawn using the Vesta software (version 3.0.2).[31]

Chemical microanalysis, especially regarding Ti and V, was done by means of X-ray energy-dispersive spectroscopy (X-EDS) in a JEOL 2000FX electron microscope equipped with an OXFORD INCA EDS detector.

Thermal analysis was performed to check stoichiometry using a TGA/DTA Netzsch STA 409 Instrument. The samples were heated at 10ºC/min to 900ºC and then held isothermally for 1 h. All the TGA/DTA experiments were performed using alumina crucibles under a flowing oxygen atmosphere with a 75 mL/min flow rate.

3. Results and Discussion

XRD patterns of the six $Li_{0.5}Ti_{1-x}V_xO_2$ samples prepared (x = 0, 0.1, 0.2, 0.3, 0.4 and 0.5) are depicted in Fig. 1. All compositions display the orthorhombic ramsdellite-type symmetry, Space Group *Pbnm*. It can be seen that in general X-ray patterns of all compositions are very similar to each other and all compositions prepared were obtained with high phase purity.

Preliminary chemical analysis carried out by EDS revealed the presence of both Ti and V for V-doped compounds. Representative EDS spectra of two samples, $Li_{0.5}Ti_{0.8}V_{0.2}O_2$ and $Li_{0.5}Ti_{0.7}V_{0.3}O_2$, are given in Fig. 2. Quantification of Ti and V were seen to be close to the nominal metals ratios for each composition.

Thermogravimetric analysis (TGA) was used to check stoichiometry and the mean Ti,V oxidation state. Samples were heated from ambient temperature to 900ºC under flowing oxygen, and the observed weight increase was used to calculate initial stoichiometry. A typical thermal analysis is shown in Fig. 3 and the main results are summarized in Table 1. $Li_{0.5}TiO_2$ (Fig. 3a) shows a maximum weight gain around 400 ºC with an incipient increase at temperatures clearly below 200ºC. The noticeable air sensitivity of $Li_{0.5}TiO_2$ would account for the slightly lower weight gain observed (4.24%) when compared to that expected for the full oxidation of Ti^{3+} (to Ti^{4+}) (4.85%), because of the inevitable handling of the sample in air before starting the TGA measurement. The weight gains observed for V-substituted $Li_{0.5}Ti_{1-x}V_xO_2$(R) are similar to that of $Li_{0.5}TiO_2$ and in agreement with the oxidation of both transition metals, Ti^{3+} and V^{3+}, to their tetravalent state. The most remarkable difference observed for $Li_{0.5}Ti_{0.7}V_{0.3}O_2$ (Fig. 3b) is the positive shift of the maximum weight gain from 350ºC (corresponding to half height of maximum weight gain) in $Li_{0.5}TiO_2$ to 650 ºC in $Li_{0.5}Ti_{0.7}V_{0.3}O_2$, indicating that V-doping in TiO_2 has a favorable effect on the thermal stability of the ramsdellite phase. That can be connected to the higher stability of V^{3+} to air/moisture. The determined mean transition metal oxidation states for all samples were in good agreement with the expected value of 3.5+ derived from their nominal composition.

Structural refinements were performed using X-ray data for all $Li_{0.5}Ti_{1-x}V_xO_2$ compounds. The structural model used in Rietveld refinements was that described previously for $Li_{0.5}TiO_2$(R) in space group *Pbnm*.[12] For all $Li_{0.5}Ti_{1-x}V_xO_2$ samples the

initial site occupancies were set according to the ideal stoichiometry of each atom type: 0.5 for Li, 1.0 for O1 and O2 sites, (1-x) Ti and x V for the same metal site, according to the respective chemical composition.

Single-crystal X-ray [12] and powder neutron diffraction studies [14] have shown that only one 4*c* channel site is occupied by lithium in $Li_{0.5}TiO_2$(R). However additional channel sites have been suggested to be occupied by lithium in ramsdellite $Li_2Ti_3O_7$ according to previous neutron diffraction studies [32-34] and entropy measurement of reaction combined with Monte Carlo simulation.[35] In order to assess the lithium site distribution in $Li_{0.5}Ti_{1-x}V_xO_2$ two compositions, x=0 and 0.3, were investigated by means of neutron diffraction. The corresponding difference Fourier synthesis maps were calculated starting from the $Ti_{1-x}V_xO_2$ skeleton framework (Fig. 4a), in which the Li channel atoms were not included (x=0.3, Fig. 4b and x=0, Fig. 4c). In both cases negative peaks for Li in the z = ¼ section were detected at a single 4*c* (x,y,¼) channel site, at coordinates $x \sim -0.06$ and $y \sim 0.47$. Lithium is readily removed from this channel site upon reaction with 1M hydrochloric acid after equation:

$$2\ Li_{0.5}TiO_2(R) + 2\ H^+(aq) \rightarrow TiO_2(R) + Li^+(aq) + H_2\uparrow$$

No noticeable residual density is detected in the difference Fourier synthesis map of the TiO_2(R) obtained after chemical lithium extraction (Fig. 4c), confirming the easiness of lithium extraction in this material.

Next, the Li atom was introduced to the structure model in the following refinements of X-ray and neutron diffraction data. After refining the profile function parameters all structure parameters of $Li_{0.5}Ti_{1-x}V_xO_2$ were allowed to vary using isotropic atomic displacement parameters. In Rietveld analysis of X-ray diffraction patterns Li parameters

from the refined neutron diffraction data of $Li_{0.5}TiO_2$ were used. No attempt was made to refine the Li structure parameters (position, temperature factor) from the X-ray diffraction data. The observed, calculated, and difference patterns for the Rietveld refinement of $Li_{0.5}Ti_{0.6}V_{0.4}O_2$ and $Li_{0.5}Ti_{0.7}V_{0.3}O_2$ using powder X-ray and neutron diffraction are shown in Fig. 5a and b, respectively. As can be seen from the patterns depicted in Fig. 5 and Fig. 1 of the supporting information (Fig. SI-1), good refinements were obtained for all samples that were seen to be of high phase purity.

The basic structural motif of ramsdellite $Li_{0.5}Ti_{1-x}V_xO_2$ are infinite double columns of edge-sharing MO_6 octahedra (M=Ti/V) running along the short *c* axis. Further corner and edge cross-linking build up a three dimensional open framework leaving channel sites that are partly occupied by lithium (Fig. 5). All samples refined satisfactorily to a simple model with one (Ti/V) framework cation 4*c* site, with occupancies according to transition metal stoichiometry for each composition, and one channel cation 4*c* site occupied by Li. Unit cell parameters obtained from X-ray and powder neutron diffraction data and the converged final R factors are presented in Table SI-1. The final atomic coordinates and isotropic atomic displacement parameters determined by Rietveld refinement are listed in Table 2. Selected bond lengths and angles are presented in Table SI-2.

The variation of normalized lattice parameters a/a_0, b/b_0 and c/c_0 with V content as extracted from X-ray data (where 0 refers to the non-doped compound) are presented in Fig. 6 together with the evolution of the unit cell volume. V-doping in TiO_2(R) produces a continuous moderate shrinking of both the large *a* and *c* edges, whereas the short *c* edge remains almost invariant (Fig. 6). As a result the unit cell volume shows a slight decrease (1.2%) with increasing V content, from 142.587(5) $Å^3$ in $Li_{0.5}TiO_2$ to 140.895(4) $Å^3$ in $Li_{0.5}Ti_{0.5}V_{0.5}O_2$. This observation is in agreement with the different ionic sizes of trivalent V (0.64 Å) and Ti (0.67 Å) in octahedral coordination [36,37], which is in line with a general

trend observed in Li_xMO_2 ramsdellites; both *a* and *b*-axis are especially sensitive probes to 1) the size of the octahedrally surrounded skeleton transition metal, M, and 2) the occupancy of the Li channel ion.[13] Both factors essentially reflect the structural flexibility of the ramsdellite structure type to accommodate different transition metals and a variant amount of Li channel ions, which are key factors with regard to lithium intercalation materials. The trend of unit cell volume for several $LiMTiO_4$ ramsdellites and analogue spinels with the size of the M^{3+} ion is illustrated in Fig. 7. For spinel (formulae per unit cell Z=8) Vol/4 has been used for a better comparison with the ramsdellite form (Z=2). Similar trends became known for $Li_{1+x}Ti_{2-2x}O_4$ ramsdellites [8] and have been quantified for the lithium insertion reaction in $LiTi_2O_4$(R) using *in situ* synchrotron diffraction.[38]

It is remarkable that V-substitution has practically no effect on the coordination environment (bond lengths and bond angles) of both $(Ti/V)O_6$ octahedra and LiO_4 tetrahedra which remain practically unaltered. No significant shift of the octahedrally centred transition metal and tetrahedrally centred lithium atom is observed and the average Ti/V-O distances are comprised between 1.992 and 1.998 Å. From neutron diffraction analysis mean Li-O distances are seen to vary between 2.038 and 2.049 Å. A perspective view of the $Li_{0.5}Ti_{1-x}V_xO_2$ ramsdellite structure is given in Fig. 8a (x=0.3) and b (x=0). The subtle tilting of edge-sharing MO_6 blocks upon lithium de-insertion is accompanied by a shrinking of the short O-O atomic distance (from 2.970 Å in $Li_{0.5}TiO_2$ to 2.852 Å in TiO_2) and a simultaneous increase of the large O-O atomic distance (from 4.835 Å in $Li_{0.5}TiO_2$ to 4.863 Å in TiO_2) of the channel window formed by oxygen atoms (Fig. 8c). The remarkable adaptability of the ramsdellite structure for lithium uptake with negligible structural changes is in the line with the excellent lithium intercalation properties such as excellent cycling stability, justified by a quasi-zero variation of the lattice constants during the lithium insertion/de-insertion reaction.

Electrochemical Li insertion properties of $Ti_{1-x}V_xO_2$ ramsdellites

The electrochemical properties of $Ti_{1-x}V_xO_2$ ramsdellites have been evaluated as the cathode in lithium half-cells. For simplicity, all materials were first completely charged yielding the fully delithiated $Ti_{1-x}V_xO_2$ ramsdellites previous to the evaluation of their electrochemical properties. Fig. 9 shows the voltage profiles of $Ti_{1-x}V_xO_2$ versus lithium studied at 25ºC and a C/30 rate in the 4.2-1V range. The discharge-charge curves show sloping profiles, roughly distributed over two voltage ranges, with a negligible voltage hysteresis during individual discharge and charge. All studied $Ti_{1-x}V_xO_2$ compositions exhibit high first discharge capacities of 270-320 mAh/g, although no one reaches the theoretical capacity (335 mAh/g) under the galvanostatic conditions used. The initial irreversible capacity decay has been attributed to the poor conductivity of TiO_2 and other titanium oxide-related materials as active materials [40] or the presence of blocking contaminants molecules impeding easy lithium diffusion into the host.[16]

After the first few cycles $Ti_{1-x}V_xO_2$ delivers constant capacities of 200-250 mAh/g. The variation of theoretical together with observed capacities during cycling is depicted in Fig. 10. In $Ti_{1-x}V_xO_2$ compounds both transition metals are in their tetravalent oxidation states. Initially lithium is inserted in the 3.0-1.7V range delivering a capacity of ca. 120 mAh/g. Afterwards insertion continues at relative lower constant voltage in the 1.7-1.0 V range where the maximum capacity is reached. The capacity displayed in the higher voltage region can be assigned to the V^{4+}/V^{3+} redox couple, whereas reduction involving the Ti^{4+}/Ti^{3+} redox couple occurs in the lower voltage region. The amount of vanadium

(x) is found to be directly related with the length of the higher voltage process (increases with x). A more detailed analysis of the discharge-charge curves during cycle no. 5 (Fig. 10) shows that theoretical capacities corresponding to the V^{4+}/V^{3+} couple are roughly reached only for low V-doped materials ($x \leq 0.2$), whereas capacities corresponding to the Ti^{4+}/Ti^{3+} redox couple deviate from their theoretical values (Fig. 10). On the other hand a decreasing mismatch to theoretical capacities is observed in high V-doped materials.

Neutron diffraction studies are now under progress to determine the exact crystal structure of highly lithiated V doped titanate ramsdellites, especially concerning the lithium channel site occupancy. On the other hand, kinetic limitations and low electrical conductivity may be an important issue in these materials, in which only ramsdellites with low V-content exhibit metallic-like behavior.[25] Good electrical conductivity is one important characteristics of a good electrode material. In this work optimization of electrode morphology (for instance using ball-milling with conductive carbon or carbon coating) has not been attempted, but may be required to achieve maximum electrochemical performances of the ramsdellite materials studied in the present work. Tailoring of the carbonaceous additives [40] used in ramsdellite titanates or synthesis using reducing atmosphere [39,41] may lead to improved capacity performances. Proper processing may be further beneficial to address the irreversible first discharge cycle capacity loss which seems to be connected to the low voltage process in these materials.

4. Conclusions

We demonstrate that vanadium doping in the TiO_2 ramsdellite structure, yielding $Ti_{1-x}V_xO_2$ ($0 \leq x \leq 0.5$), has no noticeable effect on the oxygen coordination environment of lithium as determined by neutron diffraction. The easy structural adaptability of these

materials for lithium uptake is remarkable and can be directly connected to the excellent lithium intercalation properties and cycling stability. Previously charged $Ti_{1-x}V_xO_2$ materials deliver high initial discharge capacities of 270-320 mAh/g, with a stable reversible cycling producing 200-250 mAh/g upon further cycling. Gravimetric capacities of 200-250 mAh/g (at C/50) are among the highest ever reported for a bulk intercalation compound for the threshold of 1 e^- / formula unit. The initial capacity loss observed in the first cycle is significant and may be overcome by proper electrode processing and selection of electrolyte to reach the full theoretical capacity corresponding to the intercalation of 1 Li /f.u. (335 mAh/g).

Acknowledgements

We thank Ministerio de Economía y Competividad and Comunidad de Madrid for funding the projects MAT2013-46452-C4-1-R and S-2013/MIT-2753, respectively. Financial support from Universidad CEU San Pablo is also acknowledged.

References

[1] K. M. Colbow, J. R. Dahn, R. R. Haering, *J. Power Sources* **1989**, *26*, 397-402.

[2] I. Plitz, A. DuPasquier, F. Badway, J. Gural, N. Pereira, A. Gmitter, G. G. Amatucci, *Appl. Phys. A* **2006**, *82*, 615-626.

[3] E. Ferg, R. J. Gummow, A. Dekock, M. M. Thackeray, *J. Electrochem. Soc.* **1994**, *141*, L147-L150.

[4] Y. G. Guo, Y. S. Hu, W. Sigle, J. Maier, *Adv. Mater.* **2007**, *19*, 2087-2091.

[5] T. Ohzuku, A. Ueda, N. Yamamoto, *J. Electrochem. Soc.* **1995**, *142*, 1431-1435.

[6] G. Sudant, E. Baudrin, D. Larcher, J. M. Tarascon, *J. Mater. Chem.* **2005**, *15*, 1263-1269.

[7] C. H. Jiang, M. D. Wei, Z. M. Qi, T. Kudo, I. Honma, H. S. Zhou, *J. Power Sources* **2007**, *166*, 239-243.

[8] K. Amine, I. Belharouak, Z. Chen, T. Tran, H. Yumoto, N. Ota, S.-T. Myung, Y.-K. Sun, *Adv. Mater.* **2010**, *22*, 3052-3057.

[9] A. Deschanvres, B. Raveau, Z. Sekkal, *Mater. Res. Bull.* **1971**, *6*, 699-704.

[10] A. Du Pasquier, C. C. Huang, T. Spitler, *J. Power Sources* **2009**, *186*, 508-514.

[11] D.C. Johnston, H. Prakash, Wh. Zachariasen, R. Viswanathan, *Mat. Res. Bull.* **1973**, *8*, 777-784.

[12] J. Akimoto, Y. Gotoh, M. Sohma, K. Kawaguchi, Y. Oosawa, H. Takei, *J. Solid State Chem.* **1994**, *110*, 150-155.

[13] J. Akimoto, Y. Gotoh, Y. Oosawa, N. Nonose, T. Kumagai, K. Aoki, *J. Solid State Chem.* **1994**, *113*, 27-36.

[14] R.K.B. Gover, J.T.S. Irvine, A.A. Finch, *J. Solid State Chem.* **1997**, *132*, 382-388.

[15] R.K.B. Gover, J.R. Tolchard, H. Tukamoto, T. Murai, J.T.S. Irvine, *J. Electrochem. Soc.* **1999**, *146*, 4348-4353.

[16] A. Kuhn, R. Amandi, R., F. Garcia-Alvarado, *J. Power Sources* **2001**, *92*, 221-227.

[17] E. Setiawati, M. Hayashi, M. Takahashi, T. Shodai, K. Saito, *J. Power Sources* **2011**, *196*, 10133-10140.

[18] Y. Ren, Z. Liu, F. Pourpoint, A.R. Armstrong, C.P. Grey, P.G. Bruce, *Angew. Chem. Int. Ed.* **2012**, *51*, 2164-2167.

[19] G. Armstrong, A. R. Armstrong, J. Canales, P. G. Bruce, *Electrochem. Solid-State Lett.* **2006**, *9*, A139-A143.

[20] C. Kim , R. Buonsanti , R. Yaylian , D. J. Milliron, J. Cabana, *Adv. Energy Mater.* **2013**, *3*, 1286-1291.

[21] A.R. Armstrong, G. Armstrong, J. Canales, R. Garcia, P.G. Bruce, *Adv. Mater.* **2005**, *17*, 862-865.

[22] A.R. Armstrong, G. Armstrong, J. Canales, P.G. Bruce, *J. Power Sources* **2005**, *146*, 501-506.

[23] T. Hayakawa, D. Shimada, N. Tsuda, *J. Phys. Soc. Jap.* **1989**, *58*, 2867-2876.

[24] A. Kuhn, P. Diaz-Carrasco, M. de Dompablo, F. Garcia-Alvarado, *Eur. J. Inorg. Chem.* **2007**, 3375-3384.

[25] A. Kuhn, M. Martin-Gil, F. Garcia-Alvarado, Z. *Anorg. Allg. Chem.* **2008**, *634*, 880-886.

[26] A. Kuhn, M. Martín-Gil, F. García-Alvarado, J. Solid State Chem. **2010**, *183*, 20-26.

[27] J. Rodríguez-Carvajal, *Physica B* **1993**, *192*, 55-69.

[28] M. Hoelzel, A.Senyshyn, N.Juenke, H.Boysen, W.Schmahl, H.Fuess, *Nuclear Instruments and Methods in Physics Research 2012*, *A 667*, 32-37.

[29] H. M. Rietveld, *J. Appl. Crystallogr.* **1969**, *2*, 65-71.

[30] V.F. Sears, *Neutron News* **1992**, *3*, 29-37.

[31] K. Momma, F. Izumi, "VESTA 3 for three-dimensional visualization of crystal, volumetric and morphology data," *J. Appl. Crystallogr.* **2011**, *44*, 1272-1276.

[32] B. Morosin, J.C. Mikellsen Jr, *Solid State Comm.* **1979**, *31*, 741-745.

[33] I. Abrahams, P.G. Bruce, W.I.F. David, A.R. West, *J. Solid State Chem.* **1989**, *78*, 170-177.

[34] L. Aldon, M. Van Thournout, P. Strobel, O. Isnard, J. Olivier-Fourcade, J.-C. Jumas, *Solid State Ionics* **2006**, *177*, 1185-1191.

[35] W. Cho, T. Kashiwagi, W. Ra, M. Nakayama, M. Wakihara, Y. Kobayashi, H. Miyashiro, *Electrochimica Acta* **2009**, *54*, 1842-1850.

[36] R.D. Shannon, C.T. Prewitt, *Acta Crystallogr. B* **1969**, *25*, 925-946.

[37] R.D. Shannon, *Acta Crystallogr. A* **1976**, *32*, 751-767.

[38] A. Kuhn, C. Baehtz, F. García-Alvarado, *J. Power Sources* **2007**, *174*, 421-427.

[39] A. Soares, B. Fraisse, F. Morato, C.M. Ionica-Bousquet, L. Monconduit, *J. Power Sources* **2012**, *208*, 440-446.

[40] Z. Yang, D. Choi, S. Kerisit, K. M. Rosso, D. Wang, J. Zhang, G. Graff, J. Liu *J. Power Sources* **2009**, *192*, 588-598.

[41] I. Tsuyumoto, T. Moriguchi, *Mat. Res. Bull.* **2015**, *70*, 748-752.

Table 1: Observed and expected weight gains for selected $Li_{0.5}Ti_{1-x}V_xO_2$ ramsdellites and the derived (Ti,V) oxidation state.

Nominal x	Expected weight gain (%)	Observed weight gain (%)	Observed (Ti,V) oxidation state
0	4.58	4.24	3.2+
0.3	4.53	4.30	3.4+
0.5	4.50	4.48	3.5+

Table 2: Atomic coordinates and isotropic displacement parameters *B* for ramsdellite $Li_{0.5}Ti_{1-x}V_xO_2$ ($0 \leq x \leq 0.5$) determined using X-ray and neutron diffraction data (shown in italics).

x in $Li_{0.5}Ti_{1-x}V_xO_2$						
	0	0.1	0.2	0.3	0.4	0.5
Li						
x	*-0.0508(1)*	-0.0508	-0.0508	*-0.0548(9)*	-0.0508	-0.0508
y	*0.4753(5)*	0.4753	0.4753	*0.4685(5)*	0.4753	0.4753
B	*2.0(1)*	1	1	*2.5(1)*	1	1
SOF	*0.51(1)*	0.5	0.5	*0.51(1)*	0.5	0.5
Ti/V						
x	-0.0176(6) *-0.0130(2)*	-0.0154(8)	-0.0159(8)	-0.0166(4) *-0.0158(2)*	-0.0170(7)	-0.0185(8)
y	0.1410(2) *0.1417(1)*	0.1413(3)	0.1406(3)	0.1411(1) *0.1408(1)*	0.1417(3)	0.1410(3)
B	0.12(6) *0.34(2)*	-0.14(8)	-0.06(7)	0.02(4) *0.72(2)*	0.03(7)	0.31(6)
SOF	1	0.9 / 0.1	0.8 / 0.2	0.7 / 0.3 *0.72(3)/0.28(3)*	0.6 / 0.4	0.5 / 0.5
O(1)						
x	0.7041(16)	0.7062(18)	0.6968(18)	0.6971(8)	0.7043(17)	0.7089(19)

	0.7076(1)			*0.7024(1)*		
y	0.2800(8) *0.28121(7)*	0.2812(9)	0.2786(9)	0.2785(4) *0.27928(6)*	0.2806(9)	0.2808(9)
B	1.0(3) *0.52(1)*	0.4(3)	-0.1(3)	0.3(1) *0.68(5)*	0.8(3)	0.55(14)
SOF	1	1	1	1	1	1
O(2)						
x	0.2019(13) *0.2000(1)*	0.1992(14)	0.1998(17)	0.2032(7) *0.1978(1)*	0.2032(14)	0.2067(16)
y	-0.0347(8) *-0.0366(6)*	-0.0352(9)	-0.0399(9)	-0.0380(4) *-0.03731(5)*	-0.0365(9)	-0.0368(9)
B	1.0(3) *0.33(1)*	0.4(3)	-0.1(3)	0.3(1) 0.68(5)	0.8(3)	0.55(14)
SOF	1	1	1	1	1	1

Note: All atoms in point positions 4c, ± (x, y, ¼), ± (½ - x, ½ + y, ¾)

SOF is abbreviation for site occupancy factor.

Figure Captions

Figure 1: X-ray powder diffraction patterns of $Li_{0.5}Ti_{1-x}V_xO_2$(R) (x=0, 0.1, 0.2, 0.3, 0.4 and 0.5) ramsdellite phases. Calculated peak positions are shown below the X-ray pattern corresponding to x=0.

Figure 2: X-EDS spectra of selected ramsdellites $Li_{0.5}Ti_{0.8}V_{0.2}O_2$ (a) and $Li_{0.5}Ti_{0.7}V_{0.3}O_2$ (b). Cu grids were used for the measurements.

Figure 3: Typical TGA plot showing the oxidation of $Li_{0.5}TiO_2$ (a) and $Li_{0.5}Ti_{0.7}V_{0.3}O_2$ (b) conducted in oxygen atmosphere.

Figure 4: The $Ti_{1-x}V_xO_2$ framework of $Li_{0.5}(Ti_{1-x}V_xO_2)$ ramsdellite. The unit cell is shown as black box (a). Two-dimensional difference Fourier synthesis maps of $Li_{0.5}(Ti_{1-x}V_xO_2)$ from ND patterns at the z/c = 0.25 section for x=0.3 (b) and x=0 (c). The negative residual nuclear scattering length density for the Li atom at the 4*c* channel site is clearly detected in these maps. No noticeable residual density is detected in the corresponding map after chemical lithium extraction (d).

Figure 5: Final observed (points) and calculated (solid line) X-ray diffraction (λ=1.5406 Å) pattern profile of $Li_{0.5}Ti_{0.6}V_{0.4}O_2$ (a) and neutron diffraction (λ=1.5483 Å) pattern

profile of $Li_{0.5}Ti_{0.7}V_{0.3}O_2$ (b), Space Group *Pbnm*. V_2O_3 as a minor secondary phase was included in this refinement and appears as lower vertical bars. The inset shows the ramsdellite structure along the tunnel *c* axis.

Figure 6: Evolution of the normalized lattice parameters and unit cell volume of $Li_{0.5}Ti_{1-x}V_xO_2$ with the V content x. Lattice parameters were normalized to the non-doped compound x=0.

Figure 7: Variation of the unit cell volume of $LiM^{3+}TiO_4$ ramsdellites (bottom) and analogue spinels (top) with the M^{3+} ion size. Broken lines are only used as guides to the eye. For comparison Vol/4 is used for spinel.

Figure 8: Perspective view of the $Li_{0.5}Ti_{1-x}V_xO_2$ ramsdellite structure: x=0.3 (a); x=0 (b) showing the 4-fold coordination of the Li channel ions. The fully delithiated TiO_2 is depicted in (c).

Figure 9: Discharge–charge curves of $Ti_{1-x}V_xO_2$ ramsdellites in the 4.2-1.0V range under a current density of 0.1 $mA \cdot cm^{-2}$. Selected cycles are shown.

Figure 10: Specific discharge capacities delivered upon cycling for all the $Ti_{1-x}V_xO_2$ ramsdellite compositions studied in the present work (left). The capacities for cycle no. 5 and the theoretical capacities assigned to Ti and V are shown (right).

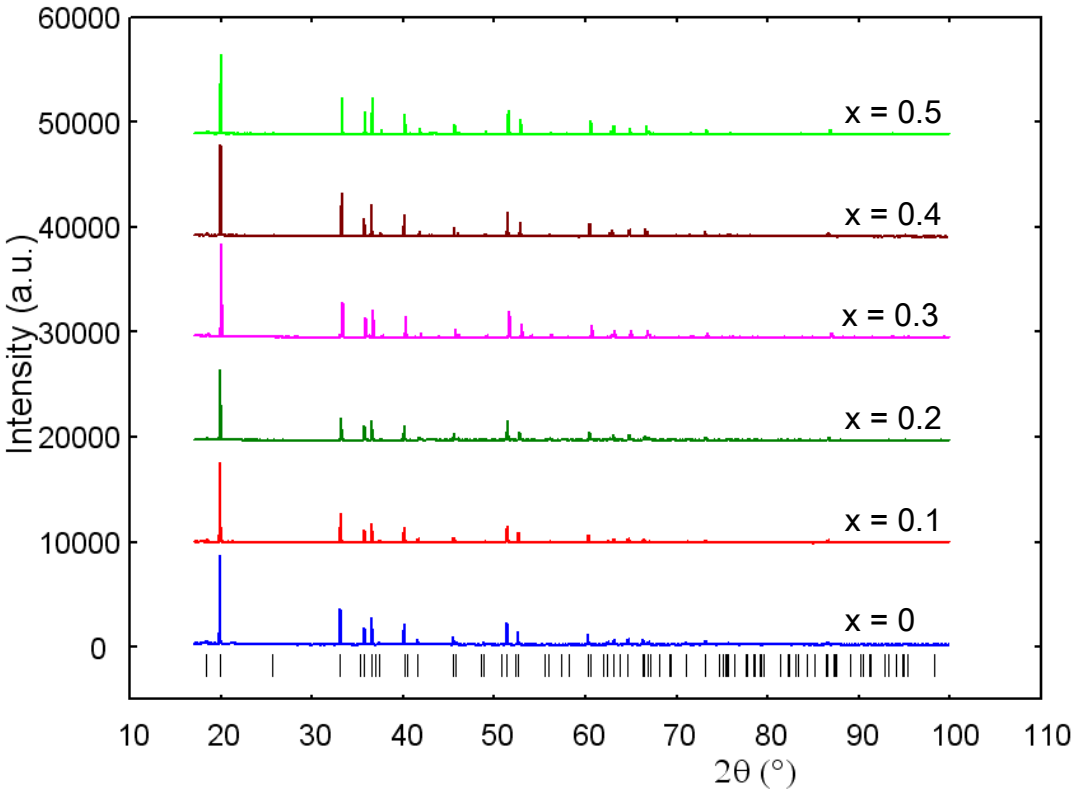
60000
50000
40000
30000
20000
10000
0
Intensity (a.u.)
x = 0.5
x = 0.4
x = 0.3
x = 0.2
x = 0.1
x = 0
10
20
30
40
50
60
70
80
90
100
110
2θ (°)

Figure 1

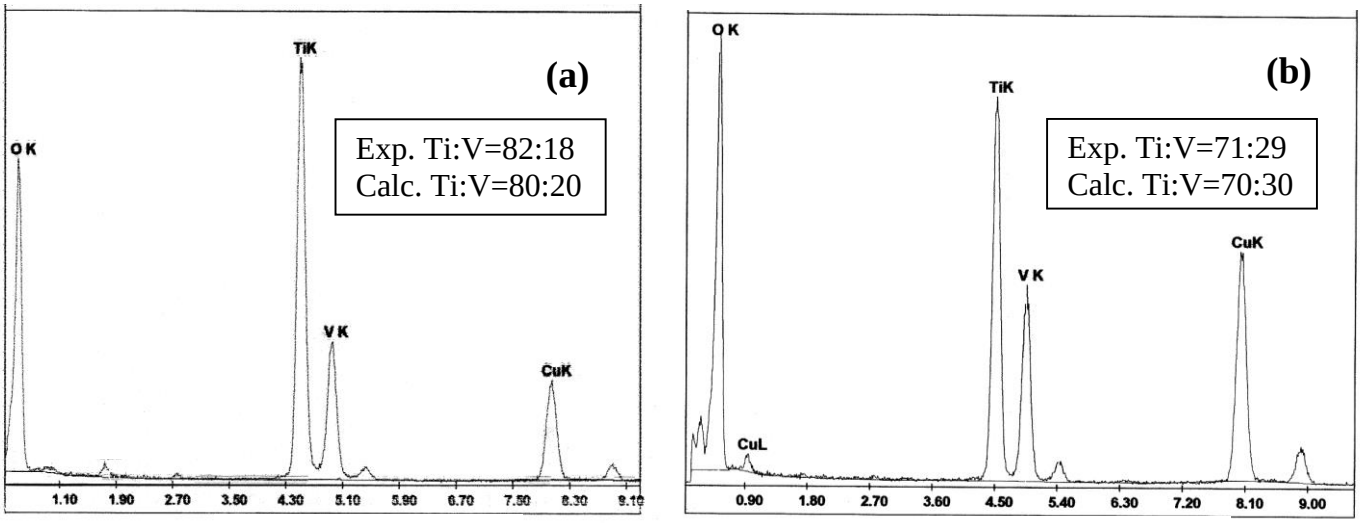
(a)
O K
TiK
V K
CuK
Exp. Ti:V=82:18
Calc. Ti:V=80:20
1.10
1.90
2.70
3.50
4.30
5.10
5.90
6.70
7.50
8.30
9.10
Energy (keV)
(b)
O K
TiK
V K
CuK
CuL
Exp. Ti:V=71:29
Calc. Ti:V=70:30
0.90
1.80
2.70
3.60
4.50
5.40
6.30
7.20
8.10
9.00
Energy (keV)

Figure 2

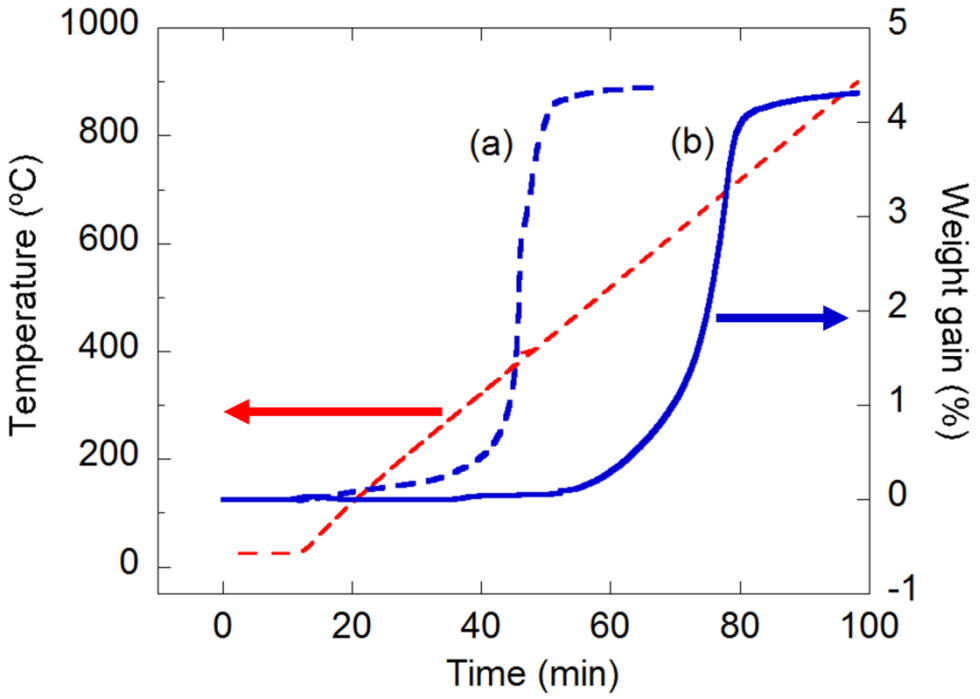
1000
800
600
400
200
0
Temperature (°C)
5
4
3
2
1
0
-1
Weight gain (%)
(a)
(b)
0
20
40
60
80
100
Time (min)

Figure 3

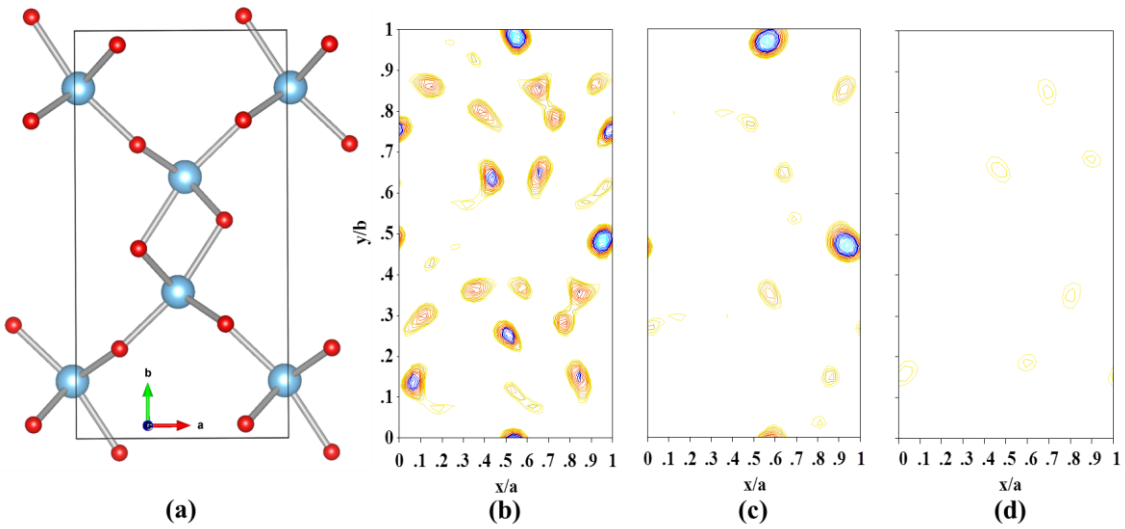

Figure 4

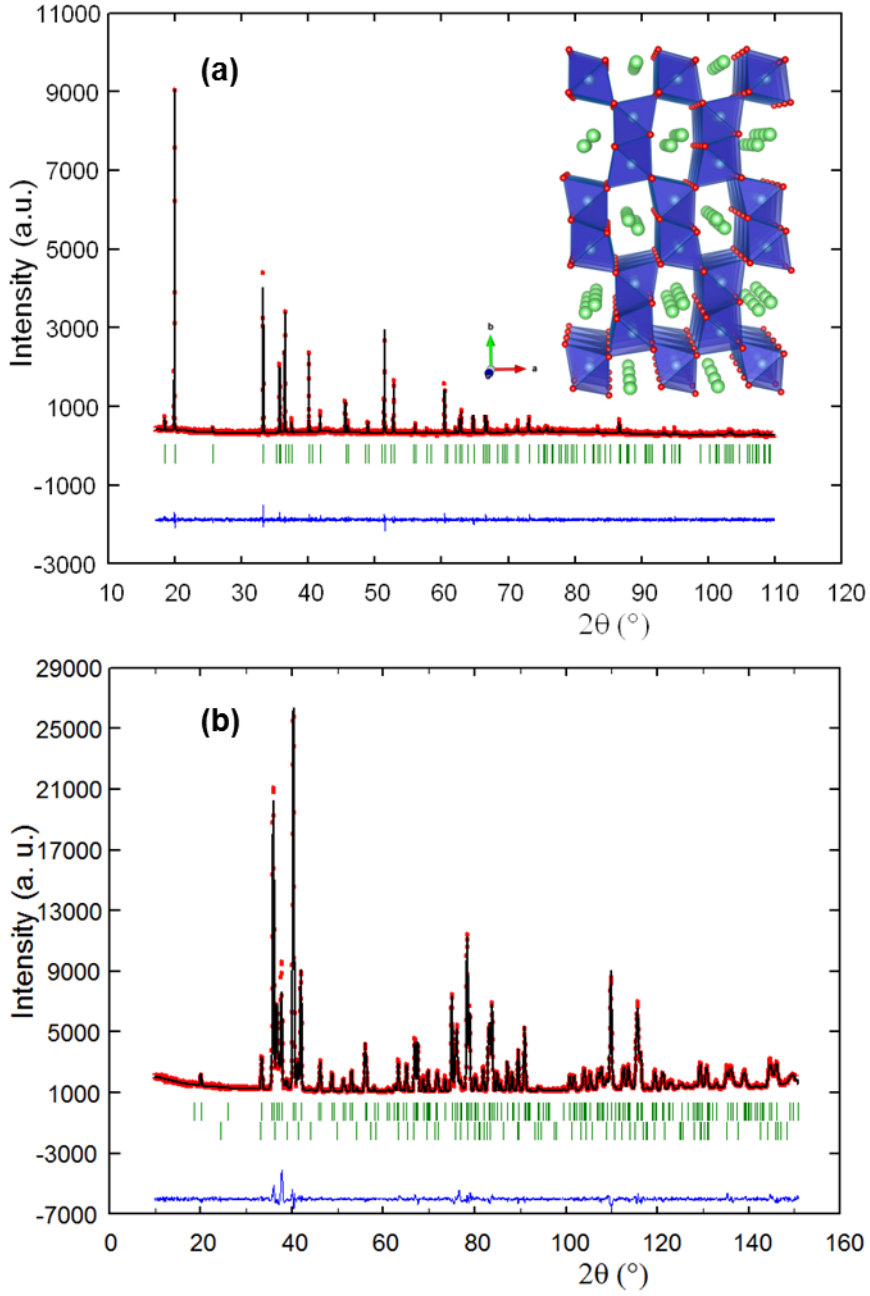
(a)
Intensity (a.u.)
2θ (°)
(b)
Intensity (a. u.)
2θ (°)

Figure 5

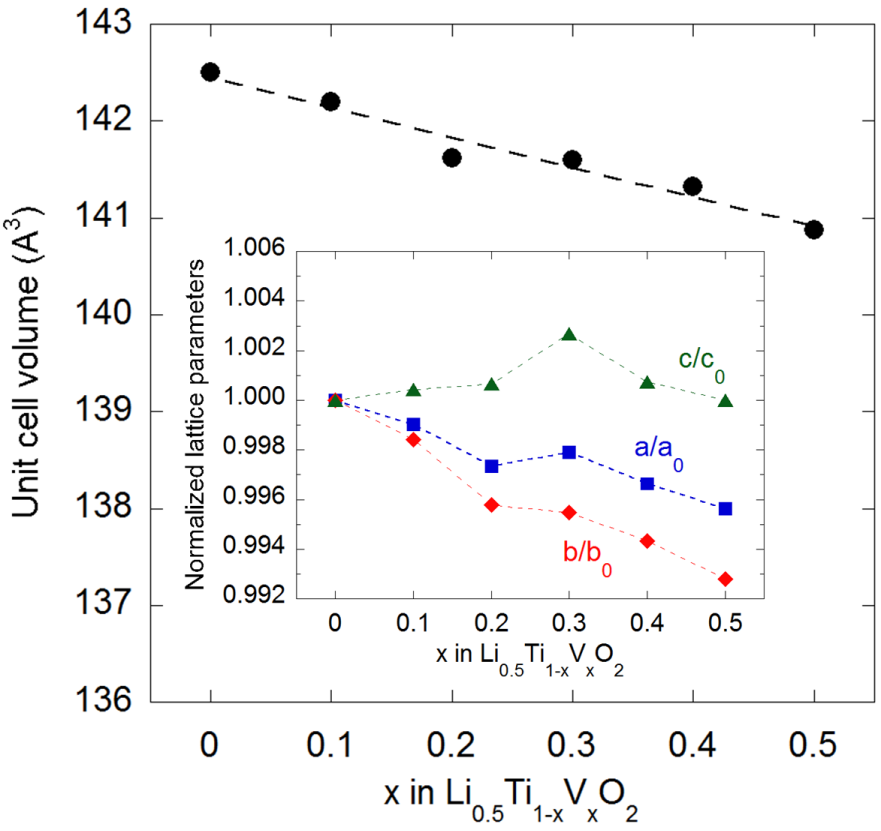

Figure 6

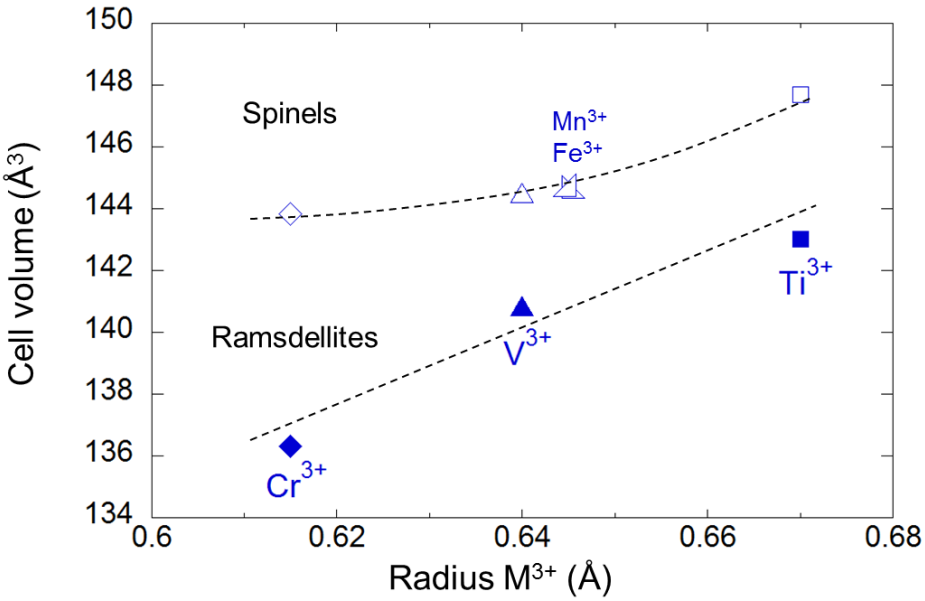
Cell volume (Å3)
Radius M3+ (Å)
Spinels
Mn3+
Fe3+
Ramsdellites
V3+
Ti3+
Cr3+
150
148
146
144
142
140
138
136
134
0.6
0.62
0.64
0.66
0.68

Figure 7

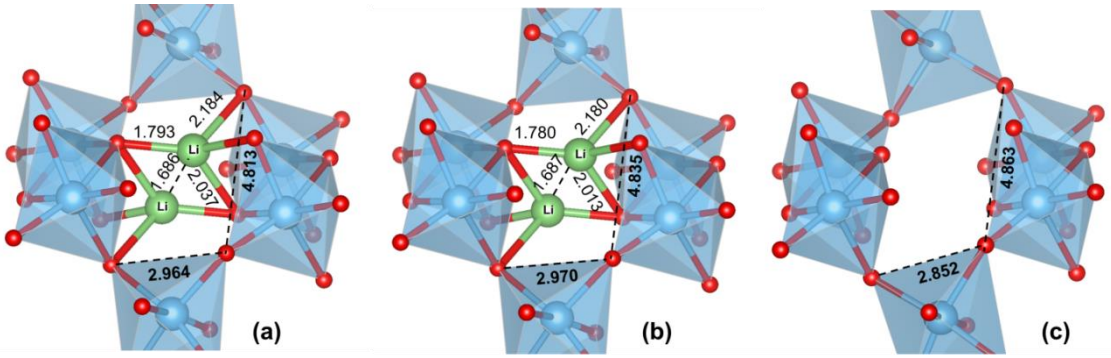
1.793
2.184
Li
1.686
2.037
Li
4.813
2.964
(a)
1.780
2.180
Li
1.687
2.013
Li
4.835
2.970
(b)
4.863
2.852
(c)

Figure 8

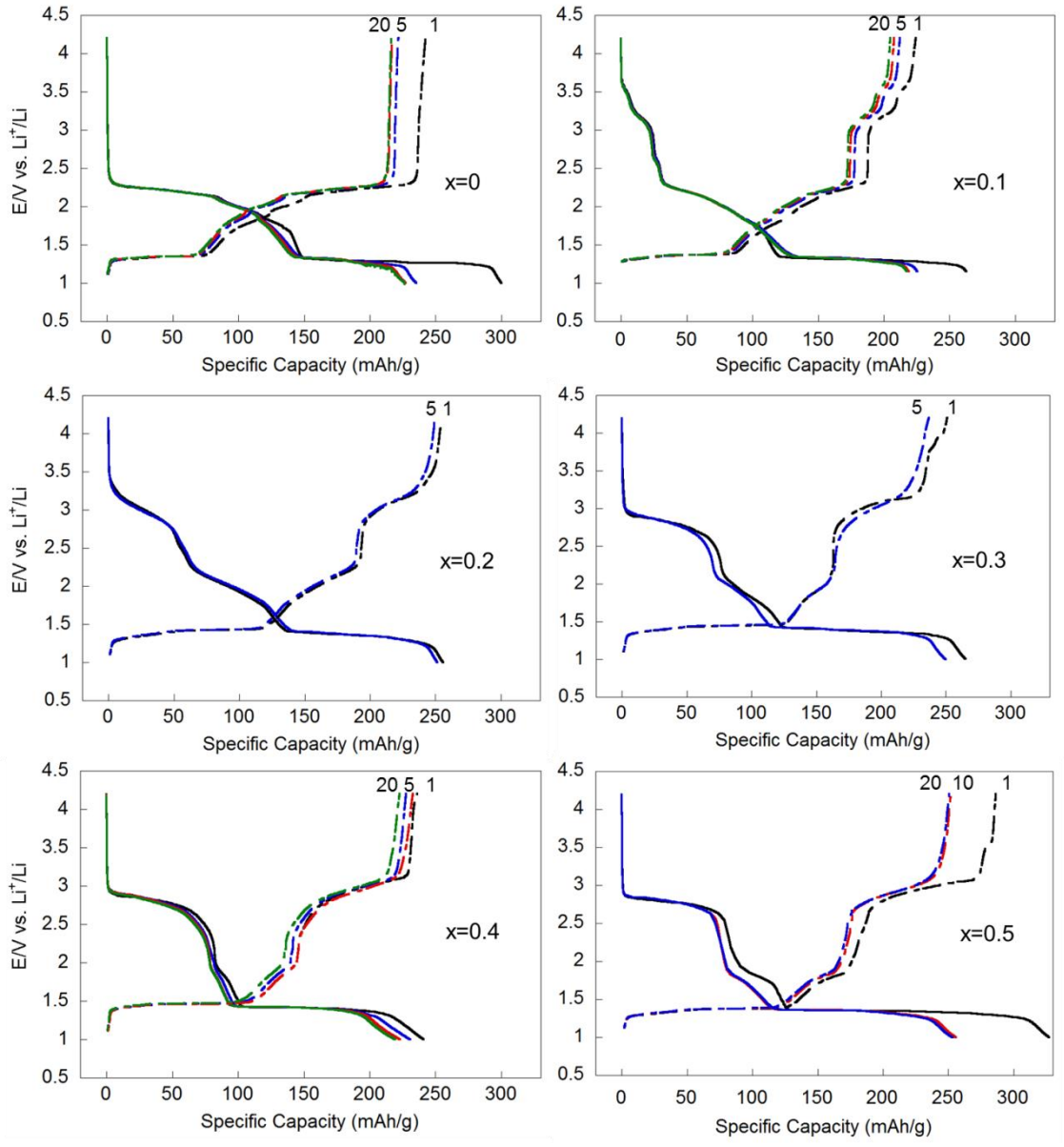
E/V vs. Li+/Li
Specific Capacity (mAh/g)
20 5 1
x=0
20 5 1
x=0.1
5 1
x=0.2
5 1
x=0.3
20 5 1
x=0.4
20 10 1
x=0.5

Figure 9

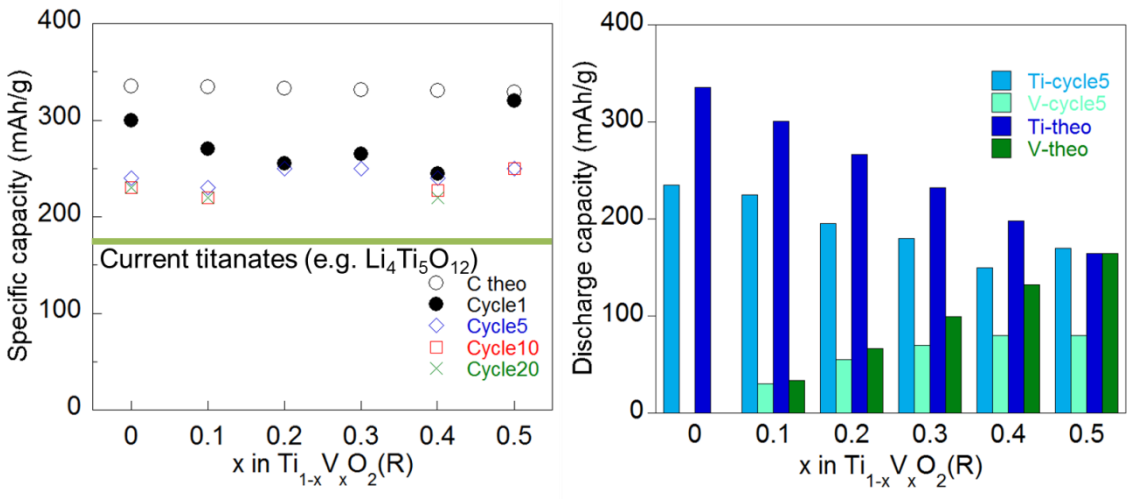

Figure 10